FULL PAPER

Dalton
www.rsc.org/dalton

Synthesis, X-ray structure, polarized optical spectra and DFT theoretical calculations of two new organic–inorganic hybrid fluoromanganates(III): $(bpaH_2)[MnF_4(H_2O)_2]_2$ and $(bpeH_2)[MnF_4(H_2O)_2]_2$ †

Pedro Núñez,*[a] Juan C. Ruiz-Morales,[a] A. D. Lozano-Gorrín,[a] Pedro Gili,[a] Vicente D. Rodriguez,[b] J. González-Platas,[c] Teresa Barriuso[d] and Fernando Rodríguez[e]

[a] *Departamento de Química Inorgánica, Universidad de La Laguna, 38200 La Laguna, Tenerife, Canary Islands, Spain. E-mail: pnunez@ull.es; Fax: 34 933318461; Tel: 34 922318501*

[b] *Departamento de Física Fundamental y Experimental, Universidad de La Laguna, 38200 La Laguna, Tenerife, Canary Islands, Spain. E-mail: pnunez@ull.es; Fax: 34 933318461; Tel: 34 922318501*

[c] *SIDIX-IUBO, Universidad de La Laguna, 38200 La Laguna, Tenerife, Canary Islands, Spain*

[d] *Departamento de Física Moderna, Universidad de Cantabria, Santander, Spain*

[e] *DCITIMAC, Facultad de Ciencias, Universidad de Cantabria, Santander, Spain*

Received 23rd September 2003, Accepted 21st November 2003
First published as an Advance Article on the web 4th December 2003

Two new fluoromanganates(III) of 1,2-bis(4-pyridyl)ethane (bpa) and *trans*-1,2-bis(4-pyridyl)ethylene (bpe), $LH_2[MnF_4(H_2O)_2]_2$ (L = bpa or bpe), have been prepared and their structure have been solved by single-crystal X-ray diffraction. The $[MnF_4(H_2O)_2]^-$ anion displays an octahedral geometry with a strong Jahn–Teller tetragonal distortion along the H_2O–Mn–OH_2 axis. The equatorial metal–ligand distances (Mn–F 1.827(1)–1.859(2) Å) are shorter than the axial ones (Mn–O 2.203(2)–2.234(2) Å). Three polarized absorption bands at 22500, 18300 and 14500 cm^{-1} are observed in the optical spectra of $(bpaH_2)[MnF_4(H_2O)_2]_2$. Finally, we present theoretical calculations on the equilibrium bond distances as well as the crystal-field electron structure using density functional methods. The calculated Mn–F bond distances (1.85 Å) are in agreement with the experimental data but the obtained Mn–O distances (2.53–2.56 Å) are higher than the experimental one as ussually found in similar Jahn–Teller distorted systems. The calculated d–d transition energies are compared with experimental energies derived from the optical spectra. The variation of the HOMO energy and transition energies against the Mn–O distance is also shown.

Introduction

The study of fluoromanganates(III) is interesting due to the wide variety of crystal structures and magnetic and optical properties exhibited by these compounds.[1–3] Mn(III) has a strong tendency to form highly distorted octahedral coordination due to the Jahn–Teller effect of the E_g electronic ground state coming from the high-spin d^4 configuration of Mn(III). These distorted octahedra can be isolated or linked in one, two or three dimensions, depending on the nature of the counter ion.[2] The final structural configuration strongly affects both the crystal anisotropy and the exchange interaction between Mn(III) thus materials properties.

Manganese(III) compounds often show a marked dichroism due to the low symmetry displayed by the manganese coordination polyhedron.[4] These effects are particularly intense in some fluoride crystals containing D_{4h} distorted $[MnF_6]^{3-}$ units.[3,5] In particular the study of the polarized optical spectra is important since the corresponding crystal-field electronic transitions are responsible for both the colour and the strong dichroism exhibited by some Mn(III) crystals.

In spite of numerous studies on fluromanganates(III) (see for example ref. 1 and references therein), there is an important lack of studies dealing with molecular modelling. This fact is likely related to the difficulty of current density functional theory (DFT) calculations to describe both the Jahn–Teller distortion and a realistic structure through a small cluster.

This work reports the synthesis, structure, polarized optical absorption spectra and theoretical calculations using DFT methods of the two new organic–inorganic hybrids: $(bpaH_2)[MnF_4(H_2O)_2]_2$, where bpa is 1,2-bis(4-pyridyl)ethane and $(bpeH_2)[MnF_4(H_2O)_2]_2$, where bpe is trans-1,2-bis(4-pyridyl)ethylene.

Experimental

Synthesis

A solution of manganese(III) oxide (0.79 g, 5 mmol, Aldrich), dissolved in hot 48% HF (20 ml) was added to a solution of (1.842 g, 10 mmol, Aldrich) bpa or (1.822 g, 10 mmol, Aldrich) bpe in 2 M HF (20 ml). Platelet crystals were grown by slow vapor–liquid diffusion of ethanol into the resulting solution at about 5 °C. Single crystals of $(bpaH_2)[MnF_4(H_2O)_2]_2$ and $(bpeH_2)[MnF_4(H_2O)_2]_2$ show a marked dichroism under a polarized optical microscope.

X-Ray diffraction

Diffraction data were collected at room temperature using a Bruker-Nonius Kappa CCD diffractometer with graphite monochromated Mo-Kα radiation. Frames were collected with the COLLECT[6] program, indexed and processed using Denzo SMN and the files scaled together using the HKL2000 program.[7] Relevant crystal data, experimental conditions and final refined parameters are listed in Table 1 for $(bpaH_2)[MnF_4(H_2O)_2]_2$ and $(bpeH_2)[MnF_4(H_2O)_2]_2$. The structure solution was obtained by direct methods, using the SIR2002 program[8] and refined using the SHELXL-97 program.[9] All non-hydrogen atoms were refined with anisotropic thermal parameters using full-matrix least-squares procedures on F^2. All hydrogen atoms were placed in geometrically idealized positions except for water and ammine hydrogen atoms that were located from

† Electronic supplementary information (ESI) available: Further calculations to verify the true minimum of the calculated structure of $[MnF_4(H_2O)_2]$. See http://www.rsc.org/suppdata/dt/b3/b311688c/

DOI: 10.1039/b311688c

Table 1 Crystal data and structure refinement for $(bpaH_2)[MnF_4(H_2O)_2]_2$ and $(bpeH_2)[MnF_4(H_2O)_2]_2$

	$(bpaH_2)[MnF_4(H_2O)_2]_2$	$(bpeH_2)[MnF_4(H_2O)_2]_2$
Empirical formula	$C_{12}H_{22}F_8Mn_2N_2O_4$	$C_{12}H_{20}F_8Mn_2N_2O_4$
M	520.20	518.18
T/K	293(2)	293(2)
λ/Å	0.71073	0.71073
Crystal system	Monoclinic	Monoclinic
Space group	$P2_1/c$	$P2_1/c$
Unit cell dimensions:		
a/Å	5.4129(10)	5.3498(10)
b/Å	18.6886(4)	18.9755(4)
c/Å	9.3323(2)	9.1497(2)
β/°	97.306(10)	95.763(10)
V/Å^3	936.39(18)	924.14(18)
Z	2	2
D_c/g cm^{-3}	1.845	1.862
μ(Mo-Kα)/mm^{-1}	1.447	1.466
Crystal size/mm	0.02 × 0.12 × 0.24	0.02 × 0.13 × 0.28
θ Range for data collection/°	2.2–28.7	2.2–28.7
Index ranges	$-7 \le h \le 5$	$-6 \le h \le 7$
	$-25 \le k \le 25$	$-25 \le k \le 25$
	$-12 \le l \le 12$	$-11 \le l \le 12$
Reflections collected/unique	16216/2413	14196/2316
R_{int}	0.034	0.063
Absorption correction	Multi-scan	
Refinement method	Full-matrix least squares on F^2	
Data/restraints/parameters	2413/0/147	2316/0/147
Final R indices [$I > 2\sigma(I)$]	$R = 0.0310$, $wR2 = 0.0854$	$R = 0.0327$, $wR2 = 0.0931$
R Indices (all data)	$R = 0.0408$, $wR2 = 0.1088$	$R = 0.0435$, $wR2 = 0.1191$
Weighting scheme, w	$1/[\sigma^2(F_o^2) + (0.0541P)^2 + 0.4051P]$	$1/[\sigma^2(F_o^2) + (0.0575P)^2 + 0.3860P]$
	$P = (F_o^2 + 2F_c^2)/3$	$P = (F_o^2 + 2F_c^2)/3$
Largest diff. peak and hole/e Å^{-3}	0.54 and −0.46	0.45 and −0.56

Fourier difference and refined isotropically. All geometric calculations were performed using the PLATON program.[10a] Molecular structures were generated using ORTEP.[10b]

CCDC reference numbers 212406 and 212407.

See http://www.rsc.org/suppdata/dt/b3/b311688c/ for crystallographic data in CIF or other electronic format.

Polarized optical spectra

A Lambda 9 Perkin Elmer spectrophotometer equipped with a Glan-Taylor polarizer was employed for recording the polarized optical absorption spectra of $(bpaH_2)[MnF_4(H_2O)_2]_2$. The quality and size of the $(bpeH_2)[MnF_4(H_2O)_2]_2$ crystals were not suitable for optical measurements.

Theoretical calculations

All the density functional calculations were carried out using the Amsterdam Density Functional (ADF) program[11] suite version 2003.01, implemented on a Compaq Server ProLiant ML530 G2. Geometry optimisations and population analysis were obtained by using functionals based on the Vosko–Wilk–Nusair (VWN)[12] form of the Local Density Approximation (LDA)[13] and on a combination (BP86) of Becke's 1988 exchange[14] and Perdew's 1986 correlation[15] corrections (Generalized Gradient Approximation GGA) to LDA and Slater-type-orbital (STO) basis set of triple-zeta quality incorporating frozen cores (O and Mn up to 1s and 3p, respectively, were kept frozen) were utilized in both restricted and unrestricted ADF calculations. Clusters centred at Mn atom involving 11 atoms (Fig. 1) have been employed in all the calculations.

Results and discussion

Two new hybrid organo–inorganic fluoromanganates(III), 1,2-bis(4-pyridylium)ethane diacuotetrafluoromanganate(III), $(bpaH_2)[MnF_4(H_2O)_2]_2$, and 1,2-bis(4-pyridylium)ethylene diacuotetrafluoromanganate(III), $(bpeH_2)[MnF_4(H_2O)_2]_2$, have been prepared from hydrofluoric solutions containing manganese and the corresponding organic base bpa or bpe, respectively. By vapor–liquid diffusion at 5 °C using ethanol as the volatile solvent crystals of these compounds were grown.

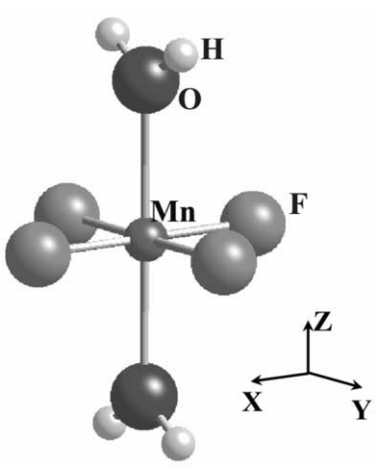

Fig. 1 Pictorial description of the 11 atom cluster used in theoretical calculations.

The asymmetric unit is constituted by one anionic octahedra $[MnF_4(H_2O)_2]^-$ and an half cation of the symmetric $(bpaH_2)^{2+}$ (Fig. 2, Table 2). The organic cations are linked to the anionic octahedral by strong hydrogen bonds, N1–H1 ··· F4 (Table 3). Manganese atoms are in an octahedral geometry with a strong Jahn–Teller tetragonal distortion along the H_2O–Mn–OH_2 axis. According to Riley's criterion,[16] we actually refer to this effect as pseudo-Jahn–Teller effect (PJTE) on dealing with heteronuclear complexes forming Jahn–Teller ions. The equatorial metal–ligand distances (Mn–F 1.827(1)–1.859(2) Å) are shorter than axial ones (Mn–O 2.203(2)–2.234(2) Å). These distances are similar to those found in other $[MnF_5(H_2O)_2]^{2-}$ and $[MnF_4(H_2O)_2]^-$ anions.[17,18]

All $[MnF_4(H_2O)_2]$ groups show approximately parallel (*ferrodistortive*) orientation of the H_2O–Mn–OH_2 axes in the

Table 2 Selected experimental bond lengths (Å) and angles (°)

	$(bpaH_2)[MnF_4(H_2O)_2]_2$	$(bpeH_2)[MnF_4(H_2O)_2]_2$
Mn–F1	1.8593(16)	1.8616(17)
Mn–F2	1.8273(14)	1.8277(16)
Mn–F3	1.8282(13)	1.8286(17)
Mn–F4	1.8473(14)	1.8433(16)
Mn–O1	2.234(2)	2.231(2)
Mn–O2	2.203(2)	2.181(3)
N1–C4	1.331(4)	1.335(4)
N1–C5	1.341(3)	1.332(4)
C1–C2	1.507(3)	1.465(4)
C1–C1	1.517(3)[a]	1.334(4)[a]
C2–C3	1.392(3)	1.388(4)
C2–C6	1.393(3)	1.397(3)
C3–C4	1.372(4)	1.367(4)
C5–C6	1.367(4)	1.371(4)
F1–Mn–F2	90.50(7)	89.92(8)
F1–Mn–F3	177.80(6)	178.30(7)
F1–Mn–F4	88.50(7)	88.59(7)
F1–Mn–O1	90.90(7)	91.94(7)
F1–Mn–O2	88.13(7)	88.07(9)
F2–Mn–F3	90.48(7)	90.85(8)
F2–Mn–F4	177.23(7)	177.19(7)
F2–Mn–O1	86.58(7)	87.20(8)
F2–Mn–O2	93.59(9)	93.62(10)
F3–Mn–F4	90.62(7)	90.70(7)
F3–Mn–O1	91.13(7)	89.61(7)
F3–Mn–O2	89.84(7)	90.37(9)
F4–Mn–O1	90.86(7)	90.47(7)
F4–Mn–O2	88.96(9)	88.71(10)
O1–Mn–O2	179.01(8)	179.19(10)

[a] $1 - x, -y, -z$.

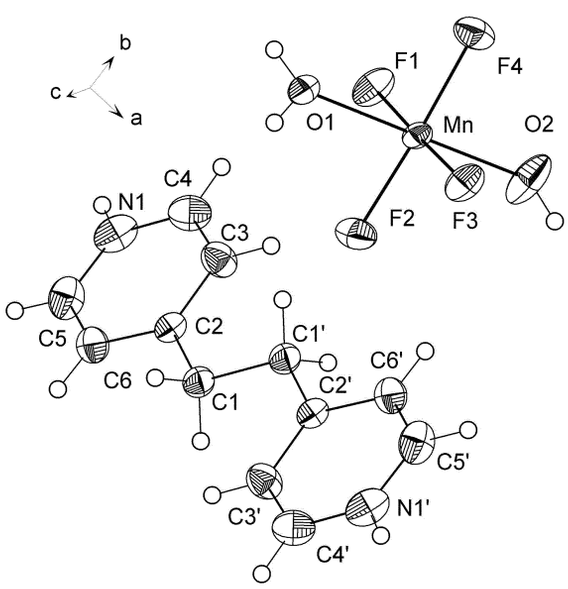

Fig. 2 ORTEP[10b] drawing of $(bpaH_2)[MnF_4(H_2O)_2]_2$ with the displacement ellipsoids at the 50% level.

plane (010) (Fig. 3). The anions are linked to a puckered 2D network in the plane (010) by the hydrogen bonds between oxygen (O1 and O2) and fluorine (F1, F2 and F3) atoms. F4 atoms are not involved in the H-bond 2D network, but connecting these layers with the organic cations, which are located in the interlayer space. The four water hydrogens are in this 2D network (Fig. 3, Table 3), with the water molecules involved in the donor function for the H-bonds.

The longest distance Mn–F1 of 1.859(2) Å correlates with the observation of two strong hydrogen bonds towards O1 and O2.[19] The cations are stacked in columns along the [100] direction and the least square planes of the bpa form with the *b* axis an angle of 29.49(4)°. The inter-ring distances between

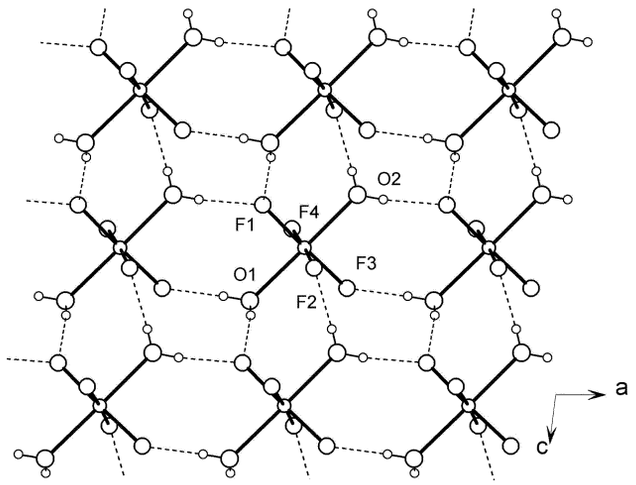

Fig. 3 2D hydrogen bonding network between the anions in $(bpaH_2)[MnF_4(H_2O)_2]_2$.

the cations corresponding to *a*/2 indicate a possible ring–ring interaction.

The structure of the $(bpeH_2)[MnF_4(H_2O)_2]_2$ crystal is similar to the previous one, with a strong Jahn–Teller effect and strong hydrogen-bond interactions (Tables 1 and 2). The structure of $(bpeH_2)[MnF_4(H_2O)_2]_2$ is similar to that shown in Figs. 2 and 3. A 2D network of hydrogen bonds as well as a *ferrodistortive* arrangement of H_2O–Mn–OH_2 formed in the plane perpendicular to the direction [010] can also be depicted for the compound containing bpe. The least square plane of bpe forms an angle of 28.19(5)° with the *b* axis. The main difference between both compounds lies the bond C1–C1′. For bpa there is a single bond (1.517(3) Å) while a double bond (1.334(4) Å) occurs for bpe. We have prepared bpe and bpa compounds since the larger rigidity provided by the bpe with respect to the bpa can lead to substantial structural differences.

The strong Jahn–Teller effect of fluoromanganates(III) is responsible for the low symmetry of the $[MnX_6]$ octahedra. Single crystals show a marked dichroism associated with this low symmetry complexes when the local distortions are cooperative. This dichroism is particularly intense in some fluoride crystals containing D_{4h} distorted $[MnF_6]^{3-}$ octahedra.[3] The highly polarized $^5B_{1g} \longrightarrow {}^5A_{1g}$ broad band occurring at around 15000 cm^{-1} is mainly responsible for the color change when the polarization plane of the light is rotated 90° around the axial F–Mn–F axis.

The polarized optical spectra of $(bpaH_2)[MnF_4(H_2O)_2]_2$ were obtained with the electric field parallel and perpendicular to the monoclinic *b* axis (Fig. 4). The optical spectra are related to the $[MnF_4(H_2O)_2]^-$ complex and are very similar to those observed

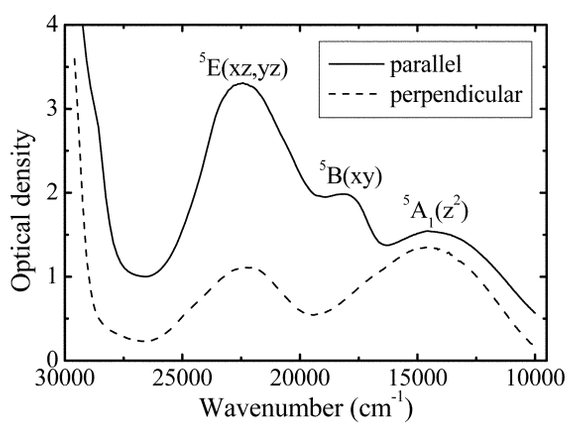

Fig. 4 Polarized optical absorption spectra of $(bpaH_2)[MnF_4(H_2O)_2]_2$ taken with the electric field parallel (continuous line) and perpendicular (dotted line) to the monoclinic *b* directions.

Table 3 Hydrogen bonds in $(bpaH_2)[MnF_4(H_2O)_2]$ and $(bpeH_2)[MnF_4(H_2O)_2]$

Donor	H	Acceptor	D ··· A/Å	D–H/Å	H ··· A/Å	D–H ··· A/°
$(bpaH_2)[MnF_4(H_2O)_2]_2$						
N1	H1N	F4[a]	2.657(2)	0.73(4)	1.98(4)	154(4)
O1	H1O1	F3[b]	2.640(2)	0.80(4)	1.85(4)	174(3)
O1	H2O1	F1[c]	2.709(2)	0.69(3)	2.02(3)	169(4)
O2	H1O2	F2[d]	2.655(2)	0.75(4)	1.91(4)	173(4)
O2	H2O2	F1[e]	2.696(3)	0.79(4)	1.91(4)	173(4)
$(bpeH_2)[MnF_4(H_2O)_2]_2$						
N1	H1N	F4[a]	2.668(3)	0.65(4)	2.09(4)	150(4)
O1	H1O1	F3[b]	2.631(3)	0.80(5)	1.83(5)	175(4)
O1	H2O1	F1[c]	2.712(3)	0.72(4)	1.99(4)	178(5)
O2	H1O2	F2[d]	2.629(3)	0.71(5)	1.92(4)	177(3)
O2	H2O2	F1[e]	2.670(3)	0.80(5)	1.88(5)	173(5)

[a] $1 + x, 1/2 - y, 1/2 + z$. [b] $x - 1, y, z$. [c] $x, 1/2 - y, 1/2 + z$. [d] $x, 1/2 - y, z - 1/2$. [e] $1 + x, y, z$.

for other Mn(III) fluoride complexes.[3] Consequently, its assignment can easily be made within a D_{4h} scheme (Fig. 5). Actually, this molecule point group is D_{2h}, but the weak equatorial distortion (Table 2) allows the complex to be treated optically as pseudo-D_{4h}. The three bands observed in the polarized optical spectra of $(bpaH_2)[MnF_4(H_2O)_2]_2$ are assigned to the spin allowed intraconfigurational d^4 transitions as $^5B_{1g}(x^2 - y^2) \longrightarrow {}^5E_g(xz,yz)$ ($\varepsilon_3 = 22500$ cm^{-1}); $^5B_{1g}(x^2 - y^2) \longrightarrow {}^5B_{2g}(xy)$ ($\varepsilon_2 = 18300$ cm^{-1}) and $^5B_{1g}(x^2 - y^2) \longrightarrow {}^5A_{1g}(z^2)$ ($\varepsilon_1 = 14500$ cm^{-1}) (Figs. 4 and 5). Here the z-axis is taken along the axial H_2O–Mn–OH_2 direction. The proposed assignment is clearly confirmed by the band polarization. According to the polarization analysis performed elsewhere,[3] the absence of the second band in the perpendicular polarized spectrum clearly indicates that the band is related to the $^5B_{2g}(xy)$ excited state.[3] In fact the $^5B_{1g}(x^2 - y^2) \longrightarrow {}^5B_{2g}(xy)$ transition is forbidden when the light polarization is parallel to the axial Mn–O direction of the complex. Values of the equatorial ligand field parameter, $10Dq(\text{eq}) = \varepsilon_2 = 18300$ cm^{-1} and the tetragonal splitting of the parent octahedral ^5E_g and $^5T_{2g}$ states, $\Delta_e = \varepsilon_1 = 14500$ cm^{-1} and $\Delta_t = \varepsilon_3 - \varepsilon_2 = 4200$ cm^{-1}, respectively, are derived from the spectra of Fig. 4 following the energy-level diagram of Fig. 5.

The values of the spectroscopic parameters corresponding to $(bpaH_2)[MnF_4(H_2O)_2]_2$, are similar to those of the $AMnF_4$ (A = K, Rb, Cs, Tl)[3] family, whose $[MnF_{4/2}F_2]$ octahedra exhibit the highest tetragonal distortion for Mn(III) ($R_{eq} = 1.84$ Å; $R_{ax} = 2.15$ Å).[17] However, while the average equatorial Mn–F distance (R_{eq}) for $AMnF_4$ is the same as that for $[MnF_6]^{3-}$ complexes and $(bpaH_2)[MnF_4(H_2O)_2]_2$, the average Mn–O distance ($R_{ax} = 2.23$ Å) in the latter one is significantly longer than the axial Mn–F distance for $AMnF_4$ ($R_{ax} = 2.15$ Å).

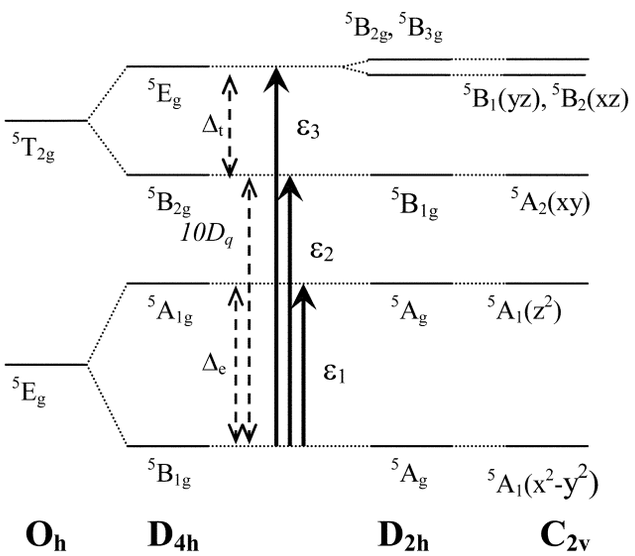

Fig. 5 State diagram showing the electronic transitions for the compounds $(bpaH_2)[MnF_4(H_2O)_2]_2$ on a D_{4h} scheme, including the levels for the related point group O_h (parent), D_{2h} and C_{2v} (not at scale).

We can compare the ligand field effects of F^- and H_2O for the same axial bond distance taking into account the optical and structural correlations established in ref. 3 for the whole fluoride series. The fact that the Δ_e and Δ_t values obtained for $(bpaH_2)[MnF_4(H_2O)_2]_2$ are similar to those for $AMnF_4$ despite the longer Mn–O axial distance was ascribed to the presence of axial water molecules.[3,5] From the empirical relations established for a series of $[MnF_6]^{3-}$ complexes[20] we can estimate the tetragonal splittings of the $[MnF_6]^{3-}$ complex having the same equatorial and axial bond distances attained in $(bpaH_2)$-$[MnF_4(H_2O)_2]_2$. The values are $\Delta_e = 18480$ cm^{-1} and $\Delta_t = 4620$ cm^{-1}.[20] Therefore, the differences between the Δ_e and Δ_t obtained for $[MnF_6]^{3-}$ and the experimental values for $[MnF_4(H_2O)_2]^-$, $\delta(\Delta_e) = 3980$ cm^{-1} and $\delta(\Delta_t) = 420$ cm^{-1}, must be associated with the stronger ligand field strength of the water molecules. Similar results are obtained for the fluoromanganates(III), $(4,4'bpyH_2)[MnF_4(H_2O)_2]_2{\cdot}2H_2O$.[5] This noteworthy result can be better understood taking into account that, within an atomic overlap model, the Δ_e parameter is given by $2[e_\sigma(\text{equatorial ligand}) - e_\sigma(\text{axial ligand})]$ where e_σ means the spectroscopic bonding σ parameter. A similar expression can be written for Δ_t in terms of the spectroscopic bonding π parameter. As the equatorial ligands are the same in $[MnF_6]^{3-}$ and $[MnF_4(H_2O)_2]^-$, the differences $\delta(\Delta_e)$ and $\delta(\Delta_t)$ can be written as $2[e_\sigma(H_2O) - e_\sigma(F)]$ and $2[e_\pi(H_2O) - e_\pi(F)]$, respectively. As a consequence, these expressions allow us to compare quantitatively the spectroscopic bonding parameters e_σ and e_π of F^- and H_2O from the atomic angular overlap model. In particular we obtain $e_\sigma(H_2O) - e_\sigma(F) = 2000$ cm^{-1} and $e_\pi(H_2O) - e_\pi(F) = 210$ cm^{-1} for $R_{ax} = 2.23$ Å, thus confirming that the σ- and π-axial interactions of the oxygen are higher than those of the fluorine following the trends of the spectrochemical series.[21]

It must be remarked that the π-bonding interaction difference $\delta(\Delta_t)$ is an order of magnitude smaller than σ-bonding interaction difference $\delta(\Delta_e)$. This result clearly reflects the relatively weakness of the π-bonding of water with respect to the σ-bonding as compared to the F ligand. The anisotropic character of the H_2O–Mn π-bonds can probably account for that difference.[22]

Table 4 shows the structural parameters of the equilibrium geometries obtained from theoretical calculations. Several types of calculations have been carried out in isolated clusters in the DFT framework (first two rows in Table 4). In all cases the

Table 4 Structural parameters of the equilibrium geometries for $[MnF_4(H_2O)_2]^-$. Experimental geometrical parameters are included for comparison

Method	Mn–F/Å	Mn–O/Å	O–Mn–O/°	F1–Mn–F2/°	F1–Mn–F3/°
ADF unrestricted	1.850–1.857	2.545	180.00	90.04	180.00
ADF restricted [a]	1.839–1.846	2.533	180.00	90.00	180.00
ADF restricted [a,b]	1.900–1.863	2.561	180.00	90.00	180.00
Experimental	1.828–1.859	2.203–2.234	179.01	90.49	177.80

[a] Taking H_2O as a fragment. [b] With four point charges in (0, ±2.11 ±3.84) positions (in Å).

geometry optimization of the $[MnF_4(H_2O)_2]^-$ molecule with the electronic configuration d^4 $\{(xz)^1(yz)^1(xy)^1(3z^2 - r^2)^1\}$ was carried out. The first and second rows in Table 4 correspond, respectively, to unrestricted and restricted calculations using ADF code in D_{2h} symmetry. In all the cases, a tetragonally elongated octahedron with different axial (Mn–O) and equatorial (Mn–F) distances was found. The calculated Mn–F bond distances using ADF program are close to the experimental values (Table 4). However the calculated Mn–O distances differ significantly from the experimental values. Similar findings were reported elsewhere.[23] The calculated and measured values of the Mn–O distances in $Li_2Mn_2O_4$, whose Mn displays a similar Jahn–Teller distortion to the $[MnF_4(H_2O)_2]^-$ anion, are 2.127 and 2.07 Å for the averaged equatorial distances whereas they are 2.497 and 2.30 Å for the "axial" distances, respectively.[24] In the quoted reference,[23] the authors suggest that the approximations inherent in the DFT calculations, as well as the restricted basis set can lead to a long axial Mn–O distance. It is also worthwhile pointing out that the use of isolated clusters could be also responsible for these results. In a previous work,[25] it was shown that the calculated distances in an isolated cluster are systematic higher than the experimental ones. The distance difference depends on the nominal charge on the central ion of the cluster, increasing from 10% in $[FeF_6]^{3-}$ to 25% in $[MnF_6]^{4-}$. According to this trend, we expect a difference of 10% in $[MnF_4(H_2O)_2]^-$, in agreement with the values shown in Table 4.

Moreover, the contribution due to the potential of the rest of the lattice can partially account for the abnormally large calculated axial distances. In order to obtain suitable values of the equilibrium distances and optical transitions on the basis of an isolated complex, the crystal electrostatic potential should be flat within the complex region. As it was not possible to include the true lattice potential in our calculations, we introduced four fictitious point charges near the water groups at (0, ±*a*, ±*b*) but the calculations carried out for different values of parameters *a* and *b* did not change essentially the calculated axial distances. The third row of Table 4 gives the calculated distances using *a* = 2.11 Å and *b* = 3.84 Å. This result confirms that a realistic "rest of the lattice" should be included in the calculations.

The calculated energies of the molecular-orbitals in D_{2h} symmetry by restricted DFT calculations are in order of increasing energy $b_{3g}(\sim yz)$ (0.433 eV), $b_{2g}(\sim xz)$ (0.505 eV), $a_g(\sim z^2)$ (0.523 eV), $b_{1g}(\sim xy)$ (0.648 eV) and $a_g(\sim x^2 - y^2)$ (2.904 eV). The HOMO (b_{1g}) is constituted by 78.5% of the d_{xy} orbital of the Mn atom, 9.7% p_x orbital and 10.8% p_y orbital of the F atom whilst the LUMO (^5A_g) consists of 66.2% of the $d_{x^2-y^2}$ orbital of the Mn atom, 13.4% p_x orbital and 12.6% p_y orbital of the F atom. From the calculated energies for the HOMO and LUMO we obtain a transition energy of 2.256 eV (18196 cm^{-1}).

Trying to explain the unexpected nature of the HOMO molecular orbital found at the theoretical equilibrium distance, the variation of the molecular orbital energies against the Mn–O axial distance has been calculated by means of restricted DFT computational methods. As can be seen in Fig. 6(a), the energies of the b_{1g}, b_{2g} and b_{3g} orbitals do not essentially change with the distance; the exception is the behaviour of a_g orbital whose energy strongly increases when the axial Mn–O distance reduces. If the experimental distance is considered, the HOMO molecular orbital is as expected mainly z^2.

Table 5 Mulliken population analysis obtained from population analysis using unrestricted DFT calculations (ADF code) for $[MnF_4(H_2O)_2]^-$

Atom	Charge	Spin density	S	P	D
Mn	1.9957	3.8183	A: −0.0293	0.0836	4.3569
			B: −0.1055	0.0333	0.6652
F (×2)	−0.7715	0.0407	A: 1.0656	2.8348	0.0056
			B: 1.0655	2.7964	0.0035
F (×2)	−0.7670	0.0440	A: 1.0685	2.8313	0.0057
			B: 1.0686	2.7892	0.0037
O (×2)	−0.5734	−0.0078	A: 0.9399	2.3244	0.0184
			B: 0.9343	2.3394	0.0168
H (×4)	0.3070	0.0070	A: 0.3001	0.0499	0.0000
			B: 0.2938	0.0492	0.0000
Total	−1	4			

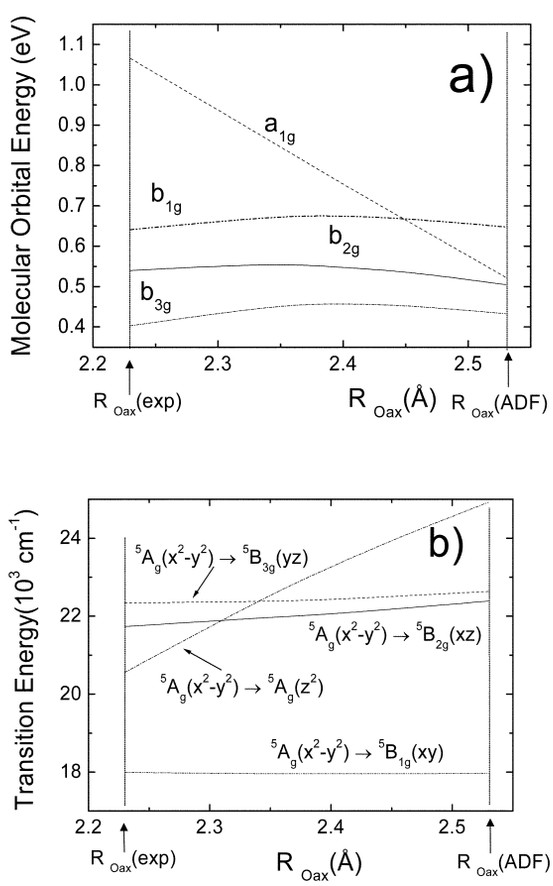

Fig. 6 Variation of (a) the calculated molecular orbital energies and (b) the intraconfigurational transition energies *vs*. axial ligand distance.

Table 5 shows the Mulliken charges calculated for each type of orbital and for each spin the atomic electron valence density using unrestricted DFT calculations. The charges for each orbital are obtained dividing the corresponding total percentage population by the number of orbitals. The results

Table 6 Energies (in cm^{-1}) of the intraconfigurational d^4 transitions for $[MnF_4(H_2O)_2]^-$ obtained by restricted DFT calculations (ADF code) at the theoretical equilibrium distances. Experimental values are also included for comparison

Transition	Calculated energy D_{2h} Symmetry	Experimental energy[a] D_{4h} Symmetry
$^5A_g(x^2 - y^2) \longrightarrow {}^5A_g(z^2)$	26743	14500
$^5A_g(x^2 - y^2) \longrightarrow {}^5B_{1g}(xy)$	17965	18300
$^5A_g(x^2 - y^2) \longrightarrow {}^5B_{2g}(xz)$	22387	22500
$^5A_g(x^2 - y^2) \longrightarrow {}^5B_{3g}(yz)$	22634	

[a] This work.

illustrate the greater importance of the d orbitals of the Mn atom and p orbitals of the F and O atoms in the studied compound. In all cases the charge on the Mn, F and O atoms are significantly smaller than the formal oxidation state and are in agreement with those of investigations of transition-metal systems.[26]

The energies of the intraconfigurational d^4 transitions have been calculated in D_{2h} symmetry by restricted computational DFT method. As a first step of approximation these transition energies were derived as the difference between the bonding energies of the ground state configuration (unoccupied $x^2 - y^2$ orbital configuration) and the excited configurations having unoccupied xy, xz, yz, and $3z^2 - r^2$ orbitals, respectively. Bearing in mind that, in D_{4h} symmetry, the $|xy\uparrow,xz\uparrow,yz\uparrow,3z^2 - r^2\uparrow|$ and $|xy\uparrow,xz\uparrow,yz\uparrow,x^2 - y^2\uparrow|$ determinants do not belong to the same irreducible representation, we have neglected, in D_{2h} symmetry, a possible interaction between these configurations both transforming in this case like A_g. It is worthwhile to mention that a similar approximation followed in the calculation of crystal-field and charge transfer transition energies in Cr^{3+} doped fluorides led to reasonable results.[27] Table 6 shows the energies for $^5A_g(x^2 - y^2) \longrightarrow {}^5B_{1g}(xy)$, $^5A_g(x^2 - y^2) \longrightarrow {}^5B_{2g}(xz)$, $^5A_g(x^2 - y^2) \longrightarrow {}^5B_{3g}(yz)$ and $^5A_g(x^2 - y^2) \longrightarrow {}^5A_g(z^2)$ d^4 transitions where, for instance, $^5A_g(x^2 - y^2)$ means a configuration having the unoccupied orbital $x^2 - y^2$ and belonging to the A_g irreducible representation. The calculated energies of the ^5A_g-$(x^2 - y^2) \longrightarrow {}^5B_{1g}(xy)$, $^5B_{2g}(xz)$ and $^5B_{3g}(yz)$ transitions show an excellent agreement with the experimental energies (Table 6). Note that the experimental $^5B_{1g}(x^2 - y^2) \longrightarrow {}^5E_g(xz,yz)$ transition in D_{4h} symmetry corresponds to the calculated $^5A_g(x^2 - y^2)$ $\longrightarrow {}^5B_{2g}(xz)$, $^5A_g(x^2 - y^2) \longrightarrow {}^5B_{3g}(yz)$ in D_{2h} scheme, which overlap in the experimental spectrum. An exception to this behaviour is the $^5A_g(x^2 - y^2) \longrightarrow {}^5A_g(z^2)$ transition, whose calculated energy exceeds more than 50% the experimental transition energy labelled as $^5B_{1g}(x^2 - y^2) \longrightarrow {}^5A_{1g}(z^2)$. However this particular transition depends strongly on the Mn–O distance as is shown in Fig. 6(b). This result contrasts with the smooth variation exhibited by the transition energies of the other three bands, which are much less sensitive to changes of the Mn–O distance. Thus a proper estimate of the $^5A_g(z^2)$ energy requires a precise account of the actual Mn–O distance. According to Fig. 6(b) the calculated energy is drastically improved upon decreasing the Mn–O distance towards the experimental equilibrium distance. This result stresses the relevance of dealing with true ligand–metal distances to account for the measured energy of certain states.

Concluding remarks

The two new fluoromanganates(III), $(bpaH_2)[MnF_4(H_2O)_2]_2$ and $(bpeH_2)[MnF_4(H_2O)_2]_2$, have been prepared and structurally characterized by XRD. The main compound difference is the single/double bond of the C1–C1′, in spite of the larger differences we expected on the basis of the rigidity of the double bond. The $[MnF_4(H_2O)_2]^-$ octahedra are distorted by a strong pseudo-Jahn–Teller effect along the H_2O–Mn–OH_2 direction and are connected by hydrogen bonds forming a layer perpendicular to the b axis. The polarized optical spectra of $(bpaH_2)[MnF_4(H_2O)_2]_2$ were explained in terms of a D_{4h} symmetry within a d^4 electronic configuration.

First DFT calculations performed on these Mn(III) heteroligand complexes are very promising as they properly account for the Mn–F equilibrium distance and also for three of the transition energies. It is worth to point out that the disagreement between the calculated and experimental values of some properties, in which the $(3z^2 - r^2)$ orbital is involved, can considerably be overcome if the experimental axial ligand distance is used in the calculations showing the relevant role played by the axial ligands.

Acknowledgements

This work was supported by the Spanish Research Program (MCYT MAT2001-3334, BFM2002-01730 and BQU2002-02794) and Canary Islands Goverment (PI 2001/53).

References

1 W. Massa, *Rev. Inorg. Chem.*, 2000, **19**(1–2), 117.
2 F. Palacio, M. C. Morón, in *Research Frontiers in Magnetochemistry*, ed. C. J. O'Connor, World Scientific, New Jersey, 1993, p. 227.
3 F. Rodriguez, P. Núñez and M. C. Marco de Lucas, *J. Solid State Chem.*, 1994, **110**, 370.
4 T. S. Davis, J. P. Fackler and M. J. Weeks, *Inorg. Chem.*, 1968, **7**, 1994.
5 P. Núñez, C. Elías, J. Fuentes, X. Solans, A. Tressaud, M. C. Marco de Lucas and F. Rodríguez, *J. Chem. Soc., Dalton Trans.*, 1997, 4335.
6 Bruker–Nonius (1997–2000): Collect Program Suite, Bruker-Nonius, The Netherlands.
7 Z. Otwinowski and W. Minor, *Methods Enzymol.*, 1997, **276**, 307.
8 M. C. Burla, M. Camalli, B. Carrozzini, G. L. Cascarano, C. Giacovazzo, G. Polidori and R. Spagna, Sir2002: A new direct methods program to solve and refine crystal structure, *J. Appl. Crystallogr.*, 2003, in press.
9 G. M. Sheldrick, SHELX-97 Release 97–2, University of Göttingen, Germany, 1998.
10 (*a*) A. L. Spek, *Acta Crystallogr., Sect. A*, 1990, **46**, C34; (*b*) C. K. Johnson, ORTEP-II: A FORTRAN Thermal Ellipsoid Plot Program for Crystal Structure Illustrations, Report ORNL-5138, Oak Ridge National Laboratory, Oak Ridge, TN, USA, 1976.
11 ADF Program System Release 2000.02, Vrije Universiteit; Theoretical Chemistry, De Boelelaan 1083; 1081 HV Amsterdam, The Netherlands, 2000.
12 S. H. Vosko, L. Wilk and M. Nusair, *Can. J. Phys.*, 1980, **58**, 1200.
13 W. Kohn and L. J. Sham, *Phys. Rev.*, 1965, **140**, A1133.
14 A. D. J. Becke, *Phys. Rev. A*, 1988, **38**, 3098.
15 J. P. Perdew and Y. Wang, *Phys. Rev. B*, 1986, **33**, 8800.
16 M. J. Riley, M. A. Hitchman and D. Reinen, *Chem. Phys.*, 1986, **102**, 11.
17 C. Elias, J. Fuentes, P. Nuñez, V. D. Rodriguez, U. Jacobs and W. Massa, *Z. Anorg. Allg. Chem.*, 1998, **624**, 2001.
18 U. Jacobs, L. Schröder, W. Massa, C. Elías, J. Fuentes, P. Nuñez and U. Bentrup, *Z. Anorg. Allg. Chem.*, 1998, **624**, 1471, and references therein.
19 W. Massa and D. Babel, *Chem. Rev.*, 1988, **88**, 275.
20 Symbols and equations were taken from ref. 3: $\Delta_e = 8.8 \times 10^4 x_D$, and $\Delta_t = 2.2 \times 10^4 x_D$, in cm^{-1}, where x_D, $= R_{ax}/R_{eq} - 1 = 0.21$; R_{eq} = average Mn–F = 1.84 Å and R_{ax} = average Mn–O = 2.22 Å. The average bond distances, R_{eq} and R_{ax}, are taken from the experimental values of $(bpaH_2)[MnF_4(H_2O)_2]_2$, leading to $\Delta_e = 18480$ cm^{-1} and $\Delta_t = 4620$ cm^{-1}.
21 See, for example: A. B. P. Lever, in *Inorganic Electronic Spectrocopy*, Elsevier, Amsterdam, 1984, pp 53–69 and 763.
22 A. Bencini, C. Benelli and D. Gatteschi, *Coord. Chem. Rev.*, 1984, **60**, 131.
23 M. Atanasov, J. L. Barras, L. Benco and C. Daul, *J. Am. Chem. Soc.*, 2000, **122**, 4718.
24 J. B. Goodenough, M. M. Thakeray, W. I. F. David and P. G. Bruce, *Rev. Chim. Miner.*, 1984, **21**, 435.
25 M. T. Barriuso, J. A. Aramburu, M. Moreno, in *Recent Advances in Density Functional Methods*, World Scientific Pub., Singapore, 2002, vol. 1, Part III, pp. 11–23.
26 A. J. Bridgeman and G. Cavigliasso, *Polyhedron*, 2000, **20**, 2269.
27 J. A. Aramburu, M. Moreno, K. Doclo, C. Daul and M. T. Barriuso, *J. Chem. Phys.*, 1999, **110**, 1497.